Metrol. Meas. Syst., Vol. 23 (2016), No. 3, pp. 425–436.

METROLOGY AND MEASUREMENT SYSTEMS
Index 330930, ISSN 0860-8229
www.metrology.pg.gda.pl

TENSILE SPLIT HOPKINSON BAR TECHNIQUE: NUMERICAL ANALYSIS OF THE PROBLEM OF WAVE DISTURBANCE AND SPECIMEN GEOMETRY SELECTION

Robert Panowicz[1)], Jacek Janiszewski[2)]

1) Military University of Technology, Faculty of Mechanical Engineering, Kaliskiego 2, 00-908 Warsaw, Poland (✉ robert.panowicz@wat.edu.pl, +48 261 837 272)
2) Military University of Technology, Faculty of Mechatronics and Aviation, Kaliskiego 2, 00-908 Warsaw, Poland (jacek.janiszewski@wat.edu.pl)

Abstract

A method of tensile testing of materials in dynamic conditions based on a slightly modified compressive split Hopkinson bar system using a shoulder is described in this paper. The main goal was to solve, with the use of numerical modelling, the problem of wave disturbance resulting from application of a shoulder, as well as the problem of selecting a specimen geometry that enables to study the phenomenon of high strain-rate failure in tension. It is shown that, in order to prevent any interference of disturbance with the required strain signals at a given recording moment, the positions of the strain gages on the bars have to be correctly chosen for a given experimental setup. Besides, it is demonstrated that – on the basis of simplified numerical analysis – an appropriate gage length and diameter of a material specimen for failure testing in tension can be estimated.

Keywords: Split Hopkinson Pressure Bar, tension testing, numerical analysis, strain-rate effects.

1. Introduction

The *Split Hopkinson Pressure Bar* (SHPB), also known as Kolsky bar, is now one of the most important methods for testing the mechanical properties of materials undergoing deformation at a high strain rate and for obtaining a constitutive relation for numerical modeling. It enables to examine materials with the strain rates from 10^2 to $5 \cdot 10^4$ 1/s.

The method foundations were developed by Kolsky in 1949 [1]. Since the days of Kolsky, who used a detonator to produce a stress pulse and condenser microphones to measure propagation of stress waves in bars, an experimental and measurement arrangement has undergone a significant modification.

Development of a classical SHPB method enabled many researchers [2–4] to test materials in the compression loading. One of the most important research, of Hauser *et al*. [5] and Lindholm [6], resulted in presenting the solutions of an experimental set-up, which are the basis of modern research equipment. They enable to characterize the dynamic behavior of different kinds of materials (metals and alloys, polymers, composites, ceramics and other) in high strain-rate conditions [7–9].

The classical SHPB method has been modified for other loading conditions. They are generally classified as the tension and torsion split Hopkinson bars methods. These modifications enable not only to specify the properties of materials in the field of high strain-rate deformation, but also to examine the process of material fractures in various stress states.

Many configurations have been developed for generating tensile loading pulses [10–15]. These methods can be divided into two groups. The first of them depends on modification

Article history: received on Nov. 02, 2015; accepted on Apr. 10, 2016; available online on Jul. 18, 2016; DOI: 10.1515/mms-2016-0027.

of the experimental arrangement for generation of a tensile input pulse. The most commonly applied method makes use of a hollow striker which slides along the incident bar and impacts the anvil to produce the tensile load, what is schematically shown in Fig. 1. The experimental apparatus was modified by Gerlach *et al*. with the use of a U shaped striker bar as a projectile [10]. The non-symmetrical striker bar makes it possible to generate a clean, without oscillation, square pulse signal five times longer than the signal typically achieved by classical striker tubes.

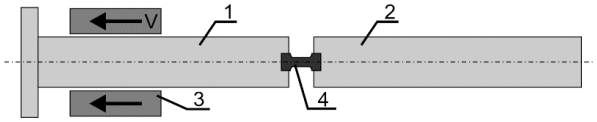

Fig. 1. A design of the tensile SHPB apparatus with a hollow striker; 1 – the incident bar; 2 – the transmitted bar; 3 – the striker impacting on the incident bar with a velocity equal to V; 4 – a specimen.

The second group for generating tensile loading pulses includes methods, which are based on the classical compression SHPB stand. In these methods, a suitable shape of a specimen in the form of a M letter [11] or a threaded specimen with a split shoulder (collar) [12] (Fig. 2) are used. The main benefit of these methods is ease of modification of a typical compression SHPB system to the configuration enabling to test materials in the uniaxial tensile state of stress. A particularly simple solution seems to be the SHPB version with a shoulder.

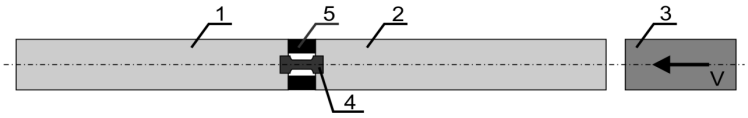

Fig. 2. A design of the tensile SHPB apparatus with a shoulder; 1 – the input bar; 2 – the output bar; 3 – the striker impacting on the output bar with a velocity equal to V; 4 – a specimen; 5 – the shoulder.

In this testing method, generation and initial transmission of a pulse are identical with those of the classical method. The compression pulse travels through the cross-section of the shoulder, the specimen and the input bar. Next, the compression pulse reflects and propagates back to the specimen as a tensile pulse. It is partly transmitted through the specimen and partly reflected. It should be noted that the shoulder does not participate in transmission of the tensile pulse since it is not connected in any way with the bars. In this way, the tensile pulse with the transmitted and reflected pulses give useful information necessary to determine the constitutive behavior of the tested material.

Referring to the theory of SHPB, associated with its name, and transmission of the useful stress pulses, the authors decided to change the bar names. The bar, in which the first useful stress wave – the tension pulse – propagates, is called the input bar, whereas the other – the output bar. In the SPHPB method with a shoulder, the compression and the transmitted pulse are traveling through the output bar.

The shoulder is made of the same material and has the same outer diameter as the bars. The inner diameter of the shoulder is large enough to mount a specimen without any contact. The cross-section area of the shoulder should be significantly greater than that of the specimen, and the shoulder outer surface should be parallel to the bar ends.

In the real experimental conditions, however, the presence of shoulder causes disturbances coming from pulse reflection from the bar-shoulder boundary surfaces. The authors' own experimental observations, as well as experiments carried out by other scientists, have shown also that, despite grinding the bars and shoulder surfaces, the wave pulse always reflects from

the boundary of the elements as a consequence of mismatch of the mechanical impedance. These disturbances may interfere with the main wave signals and cause errors in determining the stress-strain curve (see Fig. 3). To avoid such a situation, different lengths of pressure bars are usually applied. Typically, the output bar length is a double length of the input bar. Additionally, for a given bar system configuration, in order to prevent any interference with strain measurements, the location of the strain gages is chosen so as to record the wave pulses without any disturbance.

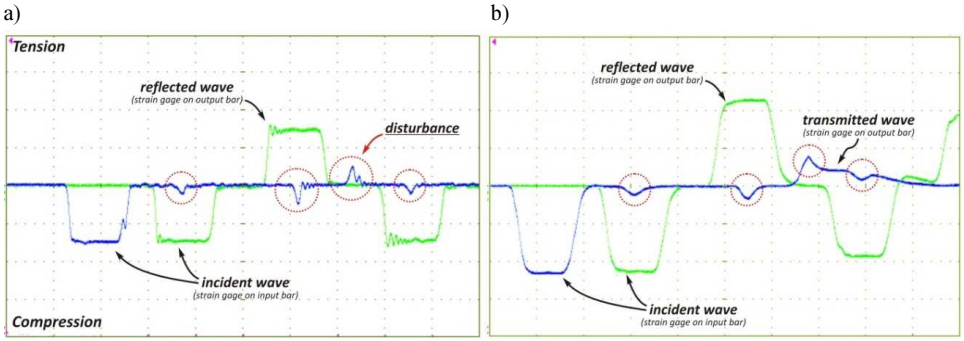

Fig. 3. The raw wave and disturbance (red circles) signals measured by the strain gages in the test configuration: a) with a shoulder only; b) with a shoulder and a specimen.

Moreover, if there is a need to study the fracture phenomena for the tested materials – especially ductile metals – it is very difficult to achieve, with the use of the above mentioned tension SHPB configuration, a sufficiently high level of plastic deformation that ensures necking and fracture of the specimen (see Fig. 4).

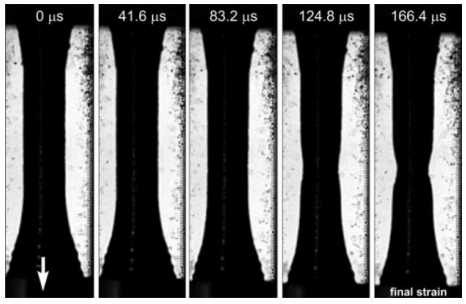

Fig. 4. The history of deformation without fracture for an armor steel specimen tested with the use of SHPB technique with a shoulder (the specimen dimensions: diameter – 3 mm, gage length – 9 mm).

It is a consequence of a limited length of striker bars usually used in conventional compression SHPB stands. As it is commonly known, the loading duration of a specimen is proportional to the striker length, which may be not sufficient to crack the specimen for its given geometry and material ductility. Therefore, it is necessary to find a suitable geometry of specimen, which will give a clean and strong enough transmitted signal and – simultaneously – will break in a given loading condition.

Due to the complexity of all the above mentioned problems, the authors made an attempt to solve them by using numerical modelling. Therefore, the paper is organized as follows: Section 2 describes the numerical model, the solution method and the tension SHPB apparatus, with the use of which the experimental verification of numerical results was performed.

The numerical data of the developed model and experimental results are collected in Section 3. The summary and conclusions are presented in the final section.

2. Methodology of numerical modelling and experiments

2.1. Numerical modelling

The authors used the Finite Element Method with a central difference time integration scheme implemented in explicit LS-Dyna to carry out the numerical simulations. This software is used to analyze various kinds of dynamic phenomena: crush, ballistic, impact, blast wave and blast wave interaction with structures, *etc*. [16].

The experimental arrangement was simplified to an axisymmetric 2D problem which enabled to analyse only bars, striker, shoulder and specimen in the axisymmetric description of the finite element model (Fig. 5). All experimental arrangement parts considered in the finite element model were meshed with the use of an axisymmetric solid volume weighted elements and hourglass control [16]. The length of the elements' side describing the bars, striker and shoulder was equal to 0.2 mm, and in the case of the specimen it was from 0.2 mm to 0.03 mm. A smaller size of the elements was given in the specimen gage section.

In the model, the real shape of threaded connection between the specimen and bars was mapped.

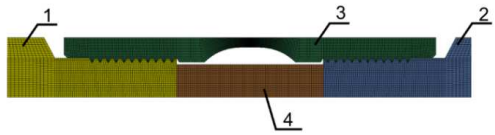

Fig. 5. A part of the Finite Element model of the considered system;
1 – the input bar, 2 – the output bar, 3 – the specimen, 4 – the shoulder.

Between the interacting surfaces, there was defined the contact based on a contact – impact algorithm, the parameters of which were established on the basis of authors' previous works [17]. A segment – to – segment method, namely the mortar method, was used to describe the contact between the surfaces. This approach was based on the projection of integration points onto the master segment with penalty regularization of contact tractions [18, 19]. For the mortar method, the contact constraints are fulfilled in a weak way. It shows the optimal convergence behavior compared to the node – to – segment methods.

The bars, striker and shoulder were made of the same material (42CrMo4 steel) defined as an elastic material with the Young's modulus E = 207 GPa, the Poisson's ratio ν = 0.3, and the density ρ = 7800 kg/m^3, which were determined based on the authors' experimental research.

In this paper, the Johnson-Cook constitutive model was applied to the specimen. The Johnson-Cook model for stress is [20]:

$$\sigma_{flow} = \left(A + B\varepsilon_p^n\right)\left(1 + C\ln\dot{\varepsilon}^*\right)\left(1 - T^{*m}\right), \tag{1}$$

where: $\dot{\varepsilon}^* = \dot{\varepsilon}/\dot{\varepsilon}_0$ is the normalized strain rate; T* is the homologous temperature given by:

$$T^* = \frac{T - T_r}{T_m - T_r}, \tag{2}$$

and other symbols mean: T – the specimen temperature; T_m – the melting temperature of the specimen; T_r – the room temperature; $\dot{\varepsilon}$ – the strain rate; $\dot{\varepsilon}_0$ – the referenced strain rate

usually equal to 1 1/s; ε_p – the plastic strain; and A, B, n, C, m are five material constants. The first bracket in the Johnson-Cook constitutive equation describes strain hardening, the second – strain rate hardening and the third – thermal softening.

The Johnson-Cook constitutive relation was complemented by the hydrodynamic equation of state in the Gruneisen form [16]:

$$p = \frac{\rho_0 C_0^2 \mu \left[1 + \left(1 - \gamma_0/2\right)\mu - a/2\,\mu^2\right]}{1 - \left(S_1 - 1\right)\mu - S_2\,\mu^2/\left(\mu+1\right) - S_3\,\mu^3/\left(\mu+1\right)^2} + \left(\gamma_0 + a\mu\right)E, \;\; \mu \geq 0\,, \tag{3}$$

$$p = \rho_0 C_0^2 \mu + \left(\gamma_0 + a\mu\right)E, \;\; \mu < 0\,, \tag{4}$$

where: $\mu = \rho/\rho_0 - 1$; ρ – the density; ρ_0 – the initial density; γ_0 – the initial value of Gruneisen gamma; a – the coefficient of the volume dependence of gamma; C_0 – the bulk sound speed; S_1 – S_3 – the Hugoniot coefficients; E – the energy per volume. The equation of state enables to perform numerical analysis with a high accuracy in situations concerning the phenomena occurring with a high strain rate, shock waves, *etc*. [16].

In order to simplify the model and shorten the time of calculations, a fracture model has not been included. It was decided that it was not required to solve the problem posed in the paper.

The material constants determining the behavior of the copper material were taken from the literature [20, 21] and are shown in Tables 1 and 2.

Table 1. The material constants of copper [20, 21].

ρ [kg/m^3]	8940	A [MPa]	99.7
E [GPa]	100	B [MPa]	262.8
ν [–]	0.31	n [–]	0.23
T_m [K]	1338	C [–]	0.029
c_p [J/(kg K)]	385	m [–]	0.98

Table 2. The EOS of copper [21].

C_0 [m/s]	3940	γ_0 [–]	2.02
S_1 [–]	1.489	a [–]	0.47
S_2 [–]	0.0	S_3 –]	0.0

The aim of the numerical analyses was to determine an optimal size of the specimens, which will enable to obtain not only relations determining the influence of strain and strain rate on flow stress, but also the influence of dynamic fracture strain.

Preliminary experimental studies performed on a classic SHPB arrangement with a shoulder, wherein the strain gages are located in a half of the bars' length, showed that the registered signals were distorted. The reflection of a compression stress pulse from the boundary between the incident bar and the shoulder as well as from the boundary between the shoulder and transmitted bars causes origination of stress pulses disturbing the measurement signals.

The disturbing signals are the result of existing a non-ideal contact (flatness and parallelism of contact surfaces) between the shoulder and the bars, despite grinding these surfaces. It resulted in a necessity of changing the position of strain gage. Therefore, the other aim of this study is to identify the places in which the strain gages should be glutted.

The numerical analysis of the high strain-rate tension was carried out for specimens with gage lengths from 2 mm to 4 mm and diameters from within the range between 2 mm and 3 mm. The compression pulse was generated by a 300 mm striker impacted at a velocity of 5 to 15 m/s. The copper specimens were examined as examples of metals characterized by high ductility (a high strain value in fracture).

2.2. Experimental set-up

In the paper, the results of numerical analyses of the main problems (signal disturbances, specimen shape and its size for tensile tests at a high strain rate) were verified experimentally with the use of a split Hopkinson pressure bar stand presented in Fig. 6. The apparatus presented in Fig. 6 was applied previously to study the dynamic properties of materials under the compression loading [2]. Due to modification of the bar system, it was adapted to the configuration for tension testing. It consists mainly of a striker launching system (air pressure gun), a striker, an input bar, an output bar (bar system), a velocity measuring device and a computer-controlled high-frequency data acquisition system.

The input bar and the output bar were 1200 and 2000 mm long, respectively, while the striker length was 300 mm. Both the bars and the striker had a common diameter of 12.0 mm and were made of 42CrMo4 steel (the nominal quasi-static yield strength $R_{0.2}$ = 1110 MPa, the sound speed C_o = 5140 m/s). Each bar was supported by linear bearing stands (4 – input bar; 6 – output bar), which were mounted on an optical bench enabling to precisely align the bar system.

The elastic deformation signals in the input and output bars were captured using a pair of strain gages attached symmetrically to the opposite surfaces of the bars. The strain gages were connected to the opposite legs of the Wheatstone bridge, which was a typical half bridge configuration. In the other legs of the bridge, the dummy resistors were mounted, the resistance of which matched the strain gages resistance. The typical electrical strain gages of 1.6 mm gage length were used (CEA-13-062UW-350, Vishay Micro Measurements). The amplified signals of the strain gages were recorded with a relatively high cut-off frequency of 1 MHz [22] with the use of a signal conditioning unit (SGA-0B V5 Wheatstone bridge with signal conditioning amplifiers, ESA Messtechnik) and a data acquisition system (LeCroy WJ354A high-speed digital oscilloscope). The strain-gage calibration was performed dynamically by measuring the velocity of the striker bar and recording the signal from the resulting pulse on both strain-gage bridges with:

$$\frac{V}{2C_0} \approx \frac{2U_0}{G_F \cdot U_I}, \tag{5}$$

where: the left side of equation expresses the amplitude of an incident wave signal predicted from the theory (V – the impact velocity; C_0 – the sound speed in bar materials), whereas the right side denotes the amplitude of an incident wave signal measured by the data acquisition system (U_0 – the voltage output; G_F – the gage factor; U_I – the bridge supply voltage).

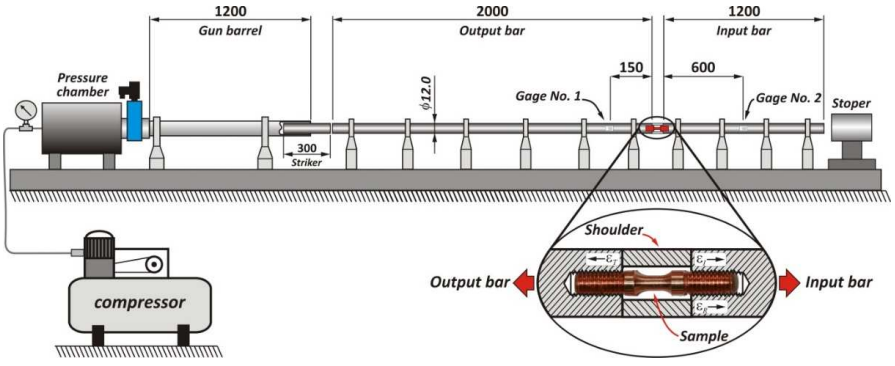

Fig. 6. A schematic diagram of the tension SHPB set-up (the recording system not shown).

3. Results and discussion

3.1. Determination of strain gage positions

The results of numerical analyses were used to determine the generation, propagation, reflection and transmission of the stress pulses in the whole considered system, with a particular reference to the measuring bars. The collinear impact of the striker produces a compression pulse in the output bar, which propagates towards the shoulder. The pulse is partly reflected from the non-ideal contact surface/boundary between the bars, and the shoulder causes mismatch of the mechanical impedance. As a result, there are created two small amplitude signals (Fig. 7), whereas the transmitted pulse reflects from the ends of the input bars and moves back to the specimen as a tensile pulse (Fig. 8). As a consequence, a complex system of waves is created in the bars, which causes interference of wave signals and disturbances.

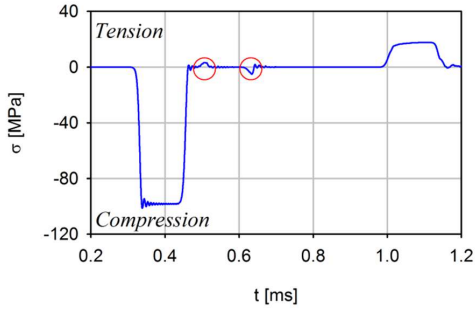

Fig. 7. The numerically obtained wave profile and disturbance (red circles) signals propagated in the output bar.

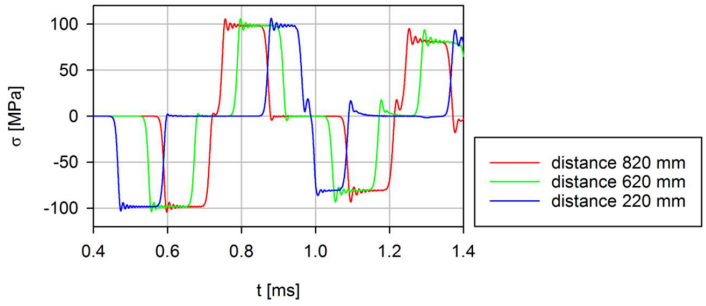

Fig. 8. The numerically obtained waves in the input bar; the distance measured from the inter-surfaces.

In order to prevent any interference with the required strain signals at a given recording moment, it is necessary to find suitable positions for the strain gages in a given setup configuration. Fig. 9 shows examples of wave profiles at different strain gage positions determined from the numerical calculations. The disturbed wave profiles are marked in blue (Fig. 9a) and in red (Fig. 9b). In turn, the undisturbed stress waves in the input bar are shown in red (Fig. 9a).

On the basis of numerical analysis, it was found that the strain gage placed on the output bar should be at a distance of 150 mm from the end which is in contact with the shoulder (Fig. 9a, red line), whereas the other strain gage placed on the input bar should be almost in the middle of the bar (620 mm from the inter-surface) (Fig. 8, green line). Such positions of the strain gages

should guarantee recording of wave signals without any disturbances resulting from application of the shoulder.

In order to confirm the above numerical results, the tests were performed. The signals recorded by the strain gages, glued at the positions determined on the basis of the numerical analysis, are shown in Fig. 10. Correctness of choosing the strain gage positions is proved by lack of interference between disturbances and a transmitted pulse. To verify whether the objectives are met, the numerical stress profile is also presented in Fig. 10, which shows a good agreement between the numerical and experimental curves for the time positions of both disturbances and wave profiles. The visible differences in shapes of compression waves and duration of transmitted waves, firstly, result from applying a 0.1-mm-thin copper pulse wave shaper which smooths the compression stress signal. Secondly, the existence of friction forces – not taken into account in the numerical modelling and resulting from an insufficient clearing of the bearings supporting the bars – extends the duration of an experimental signal in comparison to a numerical one.

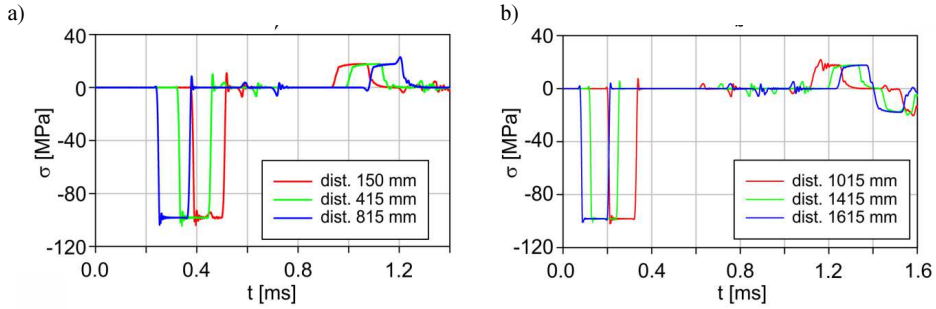

Fig. 9. The numerically obtained waves in the output bar; the distance measured from the inter-surfaces.

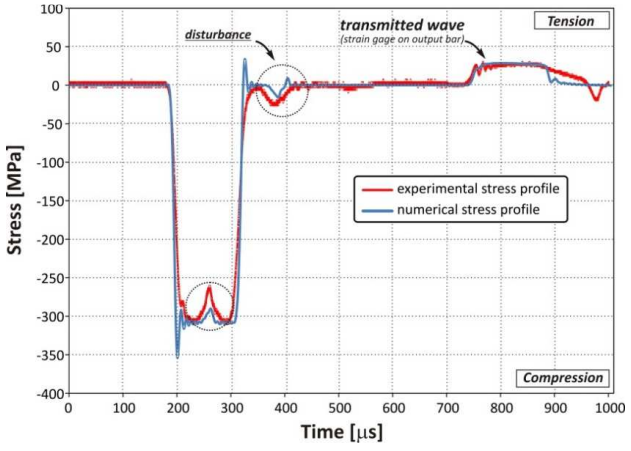

Fig. 10. The experimental raw wave and disturbance (black circles) signals measured by the strain gages glued at the positions determined with the use of numerical analysis.

3.2. Determination of specimen geometry

As it was stated before, the other main aspect presented in the paper was the problem of choosing the diameter and gage length of a material specimen enabling to test the fracture

process in metals and alloys under the dynamic loading with the use of a tensile SHPB setup with a shoulder.

At first, the history of specimen deformation in its early phase was examined. It was found that a non-ideal contact between the bars and the shoulder as well as a significant difference in the Young's modulus and yield stress values of the specimen and the bars cause origination of a small plastic deformation in the specimen after interaction with a compression pulse (Fig. 11).

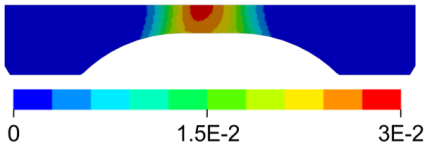

Fig. 11. The contour plots of the equivalent plastic strain in the specimen after interaction with a compression pulse.

The level of the plastic deformation depends on the pulse duration and its amplitude. It is particularly important in situations where the Young's modulus values of the specimen and the shoulder are significantly different. This problem can be overcome by applying an elastic pre-tension to the specimen.

It should be pointed out that distribution of plastic strain at the initial stage of loading is neither uniform nor symmetric relative to the central part of the specimen gage length (Fig. 12). Depending on the impact velocity, there is observed a characteristic displacement of an area of higher plastic strain in the direction of impact end of the specimen. After this initial period, the specimen is uniformly stretched until the onset of necking. The strong strain localization takes place from that moment.

To determine a gage length enabling to achieve the fracture of the specimen, nine numerical experiments were performed. The collective results of numerical analyses containing data for the considered cases are presented in Table 3. Analyzing Table 3 shows that if the impact velocity increases, the maximal strains became more and more higher for both 2 and 3 mm specimen diameters. Relatively high strains (above 0.5) for all considered gage lengths are achieved only for the impact velocity of 15 m/s, except for the 2 mm gage length, where the 0.5 strain level occurred for a lower impact velocity equal to 10 m/s. Considering the fact that the fracture strain value for copper is typically accepted as 0.5 [23], it should be assumed that a specimen with a 2 mm gage length and 2 or 3 mm diameter may fracture in the loading condition generated by the impact with a velocity exceeding 10 m/s. In turn, taking into account the machining problems of small diameter specimens (possible deformation during machining), especially those made of low strength and ductile materials, a suitable diameter of the specimen should be 3 mm. For this specimen geometry, evolution of the equivalent plastic strain is illustrated in Fig. 13.

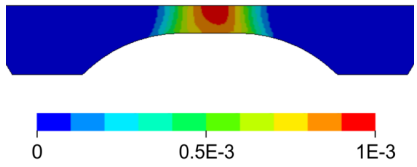

Fig. 12. The contour plots of the equivalent plastic strain at the initial stage of loading.

Table 3. The maximal strain in the specimen.

gage length [mm]	V [m/s]	ε_{max} $\phi_{specimen}$ = 2 mm	ε_{max} $\phi_{specimen}$ = 3 mm
2	5	0.25	0.19
2	10	0.75	0.51
2	15	1.92	0.98
3	5	0.165	0.15
3	10	0.495	0.39
3	15	1.25	0.75
4	5	0.13	0.11
4	10	0.33	0.29
4	15	0.82	0.57

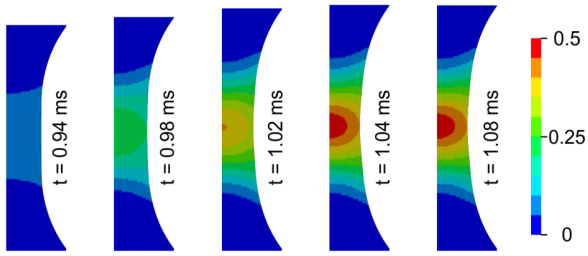

Fig. 13. Evolution of the equivalent plastic strain for a specimen with the gage length – 2 mm, the diameter – 3 mm, the striker velocity – V = 10 m/s.

Experimental verification of the conclusions resulting from numerical considerations proved correctness of the adopted assumptions. Fig. 14 shows the wave signals recorded for 3 mm diameter copper specimens with the gage lengths equal to 2 mm and 4 mm. As it can be observed in Fig. 14a, the duration of a transmitted wave signal is shorter than that of incident and reflected signals, what indicates the fracture of the specimen. For comparison, Fig. 14b presents the wave signals for a high strain-rate experiment using the specimen with a 4 mm gage length. The distinctly longer duration of the transmitted wave signal proves deformation without a fracture.

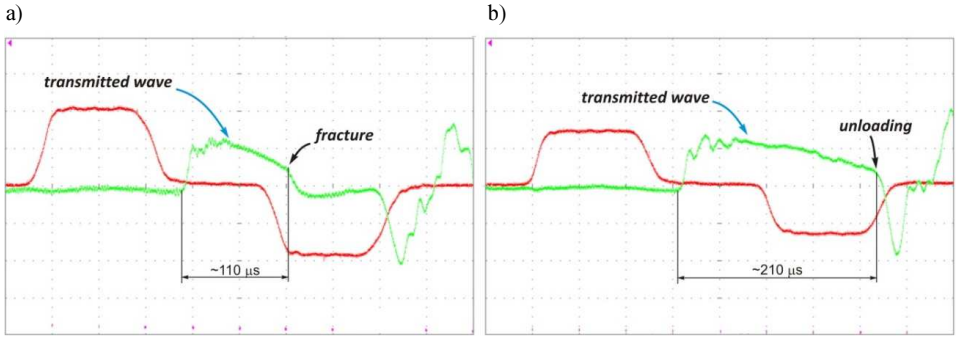

Fig. 14. The wave signals recorded for 3 mm diameter copper specimens with a gage length of a) 2 mm fracture and b) 4 mm – no-fracture.

4. Conclusions

In the presented paper, the authors focused on analyzing the tension SHPB in the aspect of selecting the strain gage location and the specimen's shape.

An experimental arrangement of the tension SHPB with a split shoulder was examined. In this solution, the proper position of strain gages should be found, regarding the disturbances caused by the impedance mismatch. It appeared that at the considered lengths of the bars and the striker, the strain gages on the output bar should be placed at a distance of 150 mm from the end which is in contact with the shoulder, whereas on the input bar they should be placed almost in the middle of the bar (620 mm from the inter-surface). On the ground of the travelling pulses and the disturbing in the bars, a greater margin of error is observed for the input bar than for the output bar.

Taking into account the problems with machining of small diameter specimens and the necessity of finding the specimen geometry which ensures its fracture in typical experimental conditions, it was proved that the specimens should have a diameter of 3 mm and the gage length – 2 mm. In such a situation, a 300 mm long striker should be propelled to about 10 m/s.

The results presented in the paper were based on the numerical analyses supported by experimental verification. The tests confirmed both the assumptions adopted in calculations and their results.

Acknowledgements

This work was partly supported by the National Centre for Research and Development (Grant No. DOBR-BIO4/031/13249/2013).

References

[1] Kolsky, H. (1949). An investigation of the mechanical properties of materials at very high rates of loading. *Proc. Phys. Soc. Lond.*, B 62, 676–700.

[2] Baranowski, P., Janiszewski, J., Malachowski, J. (2014). Study on computational methods applied to modelling of pulse shaper in split-Hopkinson bar. *Arch. Mech.*, 66, 6, 429–452.

[3] Kruszka, L., Magier, M., Zielenkiewicz, M. (2014). Experimental analysis of visco-plastic properties of the aluminium and tungsten alloys by means of Hopkinson bars technique. *Applied Mechanics and Materials*, 566, DOI:10.4028/www.scientific.net/amm.566.110.

[4] Moćko, W. (2014). The influence of stress-controlled tensile fatigue loading on the stress-strain characteristics of AISI 1045 steel. *Materials & Design* 58, 145–153.

[5] Hauser, F.E., Simmons, J.A., Dorn, J.E. (1961). Strain rate effects in plastic wave propagation. *Response of Metals to High Velocity Deformation*. Shewmon, P.G., Zackay, V.F., (ed.), New York: Interscience, 93–114.

[6] Lindholm, U.S. (1964). Some experiments with the split Hopkinson pressure bar. *J. Mech. Phys. Solids*, 12, 317–335.

[7] Owens, A.T., Tippur, H.V. (2008). A Tensile Split Hopkinson Bar for Testing Particulate Polymer Composites Under Elevated Rates of Loading. *Exp. Mech.*, 49(6), 799–811.

[8] Field, J.E., Walley, S.M., Proud, W.G., Goldrein, H.T., Siviour, C.R. (2004). Review of experimental techniques for high rate deformation and shock studies. *Int. J. of Impact Engineering*, 30, 725–775, DOI:10.1016/j.ijimpeng.2004.03.005.

[9] Cadoni, E., Solomos, G., Albertini, C. (2009). Mechanical characterization of concrete in tension and compression at high strain rate using a modified Hopkinson bar. *Mag. Concrete Res.*, 61, 221–228.

[10] Gerlach, R., Kettenbeil, Ch., Petrinic, N. (2012). A new split Hopkinson tensile bar design. *Int. J. of Impact Engineering*, 50, 63–67.

[11] Mohr, D., Gary, G. (2007). M-Shaped specimen for the high-strain rate tensile testing using a split Hopkinson pressure bar apparatus. *Exp. Mech.*, 47, 681–692, DOI:10.1007/s11340-007-9035-y.

[12] Nicholas, T. (1981). Tensile testing of materials at high rates of strain. *Exp. Mech.*, 21, 177–185, DOI:10.1007/BF02326644.

[13] Lindholm, U.S., Yeakley, L.M. (1968). High Strain-rate Testing: Tension and Compression. *Exp. Mech.*, 8(1), 1–9.

[14] Staab, G.H., Gilat, A. (1991). A direct-tension split Hopkinson bar for high strain-rate testing. *Exp. Mech.*, 31(3), 232–235.

[15] Ogawa, K. (1984). Impact-tension compression test by using a split-Hopkinson bar. *Exp. Mech.*, 24(2), 81–86.

[16] Hallquist, J.O. (2005). *Ls-Dyna Theory Manual*. Livermore Software Technology Corporation, Livermore.

[17] Panowicz, R. (2013). Analysis of selected contact algorithms types in terms of their parameters selection. *Journal of KONES Powertrain and Transport*, 20(1).

[18] Konyukhov, A., Schweizerhof, K. (2013). *Computational contact mechanics, geometrically exact theory for arbitrary shaped bodies, Lecture notes in applied and computational mechanics*. Springer, DOI: 10.1007/978-3-642-31531-2.

[19] Fischer, K.A., Wriggers, P. (2006). Mortar based frictional contact formulation for higher order interpolations using the moving friction cone. *Computer Methods in Applied Mechanics and Engineering*, 195, 5020–5036.

[20] Johnson, G.R., Cook, W.H. (1983). An constitutive model and data for metals subjected to large strains, high strain rates and high temperatures. *7th International Symposium on Ballistics*, 541–547.

[21] Steinberg, D.J. (1996). *Equation of State and Strength Properties of Selected Materials*. LLNL Report no. UCRL-MA-106439.

[22] Moćko, W. (2013). Analysis of the impact of the frequency range of the tensometer bridge and projectile geometry on the results of measurements by the split Hopkinson pressure bar method. *Metrol. Meas. Syst.*, 20(4), 555–564.

[23] Johnson, G.R., Cook, W.H. (1985). Fracture characteristics of three metals subjected to various strains, strain rates, temperatures and pressures. *Engineering Fracture Mechanics*, 21(1), 31–48.